JCS–Japan

FULL PAPER

Hydrothermal synthesis of near-monodisperse iron oxide nanoparticles using an ammonia-treated Fe-oleate precursor

Yuki Makinose[1],†

[1]**Graduate School of Natural Science and Technology, Shimane University, 1060 Nishikawatsu-cho, Matsue 690–8504, Japan**

This paper discusses the hydrothermal synthesis of monodisperse oleate-capped iron oxide nanoparticles from an ammonia-treated Fe-oleate precursor solution. Nanoparticle samples synthesized at different temperatures were characterized using a combination of X-ray diffraction, Fourier-transform infrared spectroscopy, transmission electron microscopy, dynamic light scattering, vibrating sample magnetometry, and thermogravimetry-differential thermal analysis. This characterization revealed nanoparticles comprising inverse-spinel-type crystals covered by an oleate double-layer, with the saturation magnetization of the nanoparticles increasing with the temperature used for hydrothermal synthesis. Near-monodisperse nanoparticle distributions were obtained with hydrothermal reactions conducted at 150 °C.

1. Introduction

Because of their uniform size and magnetic properties, monodisperse iron oxide nanoparticles are used as hyperthermia agents, drug delivery systems, data storage devices, and biosensors. Here, a distribution is described as monodisperse if its coefficient of variation (CV), calculated as the ratio of the standard deviation of the population's particle size to the average particle size, is lower than 10 %. Syntheses of monodisperse nanoparticles require aggregation prevention (for example, by including a surfactant in the precursor solution or adjusting the pH of the precursor solution), uniform nucleation, and crystal growth. Monodisperse iron oxide nanoparticles are typically synthesized using thermal decomposition processes, which require an Fe-organic complex, high-boiling-point organic solvents, and additives such as oleic acid or oleylamine.[1)–7)] However, the development of processes employing inorganic solvents is important for reducing the negative environmental effects of nanoparticle synthesis. Although the subcritical hydrothermal synthesis of nanoparticles from aqueous solutions is well-established,[8)] iron oxide nanoparticles produced using such techniques are not strictly monodispersed. The polydispersity of the resulting nanoparticle distribution is considered a result of non-uniform particle growth, caused by the poor dispersal of the Fe-organic precursor in aqueous solution. This paper reports the successful synthesis of distributions of iron oxide nanoparticles with low CVs using a hydrothermal method. This synthesis is enabled by the use of a hydrophilic, alkali-treated Fe-oleate precursor. The temperature at which the hydrothermal reaction is conducted affects the crystallinity, crystal growth, and magnetic properties of the nanoparticles, with higher temperatures leading to improved crystallinity and magnetic properties and larger nanoparticle sizes. Conversely, a lower temperature reduces the cost of nanoparticle synthesis. For instance, a closed container is not required for reactions conducted at 80 °C. Thus, the effect of hydrothermal temperature on the CVs of distributions of iron oxide nanoparticles was investigated at 80–200 °C.

2. Experimental section

To prepare iron oxide nanoparticles using the hydrothermal method, 5 mmol of $FeCl_2 \cdot 4H_2O$ (FUJIFILM Wako Pure Chemical Co., Guaranteed reagent) was dissolved in 10 mL of distilled water, while 5 mmol of sodium oleate (Nacalai Tesque, Inc., Extra pure reagent) was dissolved in 20 mL distilled water; this created an $FeCl_2$ solution and a sodium oleate solution, respectively. The sodium oleate solution was subsequently mixed into the $FeCl_2$ solution under agitation to form a white-brown precipitate. Next, the supernatant of this mixture was separated from the precipitate by suction filtration, conducted using a 10.0 μm polytetrafluoroethylene (PTFE) membrane. Following this, the precipitate was washed three times with distilled water, then removed from the wash solution via suction filtration for 3 min. This washing process was employed to ensure good reproducibility of synthesis. Under agitation, 5 mL

† Corresponding author: Y. Makinose; E-mail: makinose@riko.shimane-u.ac.jp

of a 28 % aqueous ammonia solution (FUJIFILM Wako Pure Chemical Co., Guaranteed reagent) was mixed with the precipitate, and the separated supernatant was added dropwise into the precipitate. The resulting mixture was subsequently placed in a PTFE vessel within a stainless-steel autoclave. Hydrothermal treatment was conducted for 6 h at 200, 150, 100, or 80 °C in an electric oven. Incubated samples were subsequently centrifuged at 4500 rpm for 10 min, after which, the supernatant was removed, and dried overnight at 60 °C. Following this, cyclohexane was added to the dry sample. This mixture was then centrifuged at 4500 rpm for 20 min, and the resulting supernatant was dried overnight at 20–22 °C. Nanoparticle samples were labelled according to the temperature of the hydrothermal reaction (e.g., Mag200 refers to the sample obtained for the reaction conducted at 200 °C). Some dried nanoparticle samples were stored in cyclohexane, where they exhibited good dispersion for several weeks after synthesis.

Nanoparticle samples were characterized using a combination of techniques. Powder X-ray diffraction (XRD) for identifying the crystal structure of the samples was performed with the Rigaku SmartLabXE, using Co Kα radiation. Fourier-transform infrared (FT-IR) spectroscopy was conducted with a JASCO FT/IR-4600 spectrometer, using the KBr plate method. Transmission electron microscopy (TEM) was performed using a JEOL JEM-2010 microscope for analyzing the size distributions of the nanoparticles under dry conditions. Here, a liquid sample of nanoparticles dispersed in cyclohexane was dropped onto an elastic carbon-support film and dried. The number and sizes of the particles in each sample were determined from the resulting TEM images using ImageJ software.[9] Selected area electron diffraction (SAED) patterns for additional analysis of the crystal structure of the iron oxide samples were obtained from the TEM images using the ReciPro software program. The size distribution of the nanoparticles in solution was analyzed by dynamic light scattering (DLS), performed with a Horiba LB-550 system. The magnetization curves of the iron oxide nanoparticles were measured using vibrating sample magnetometry (VSM), performed with a BHV-50 magnetometer (Riken Denshi Co., Ltd.). Thermogravimetry-differential thermal analysis (TG–DTA) measurements were conducted under air flow at a heating rate of 10 °C/s using the Rigaku TG–DTA8122 tool.

3. Results

The crystal phases of the nanoparticle samples were identified using XRD; the patterns obtained for the samples synthesized at each temperature are shown in **Fig. 1**. The correspondence of these patterns to that of AMCSD 00-900-2673 suggests the synthesis of crystals of Fe_3O_4, or similarly structured γ-Fe_2O_3. Although determining the exact iron oxide composition of the nanoparticles using this information is difficult because of their small crystallite sizes, Mössbauer spectroscopic measurements indicate behavior different from that of bulk Fe_3O_4 (see Supporting
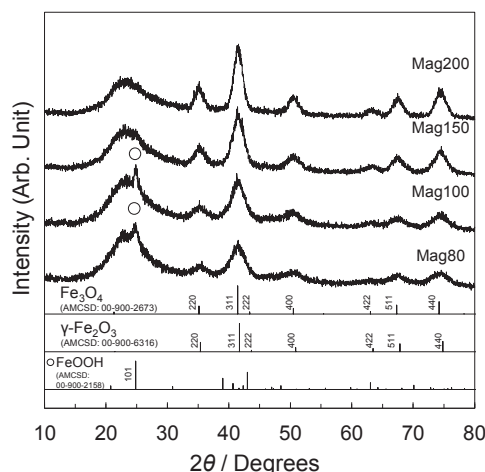

Fig. 1. XRD patterns of iron oxide nanoparticles synthesized at different temperatures with the hydrothermal method.

Information). The XRD patterns indicate that the nanoparticles have an inverse-spinel-type structure. An FeOOH phase was observed in the Mag100 and Mag80 samples. The large peak at approximately 25° was attributed to the glass holder. After fitting the patterns to a Gaussian curve, the crystallite sizes of the samples were calculated based on the sizes of their 311 peaks using the Debye–Scherrer equation. Hence, the crystallite sizes of the Mag200, Mag150, Mag100, and Mag80 samples were estimated to be 5.9, 4.6, 3.9, and 3.8 nm, respectively.

The potential generation of Fe_3O_4 or γ-Fe_2O_3, even though only Fe^{2+} was used as the source material, indicates that the oxidation of Fe^{2+} occurs during the hydrothermal process. The Fe-oleate precursor turned brown upon exposure to air during suction filtration. In contrast, when protected from air, it remained white and brown, suggesting that almost all Fe^{2+} ions in this region were maintained as Fe^{2+}. The Fe-oleate precursor was modified by the addition of the aqueous ammonia solution, with the precipitate gradually changing color to green, then black, and finally, brown. This sequence indicates that the inclusion of the aqueous ammonia solution is the primary cause of Fe^{2+} oxidation. The color of the final product was black, corresponding to the typical color of Fe_3O_4/γ-Fe_2O_3 solutions. The samples showed good dispersibility in the aqueous ammonia reaction solution.

Figure 2 shows the FT-IR spectrum of the Mag200 sample as a representative result of the spectroscopic analysis conducted to determine the organic content of the nanoparticle samples. All other FT-IR spectra displayed similar features. As oleate-capped iron oxide nanoparticles have been characterized in previous studies,[1),8),10),11)] the results of our FT-IR analysis can be explained using observations from the literature. Here, the elevated baseline of the curve is caused by the sample's scattering of infrared light. The broad band at 597 cm^{-1} corresponds to vibration of the Fe–O bond,[12] while the bands at 1456 and 1576 cm^{-1} correspond respectively to the symmetric and asymmetric stretching of COO$^-$.[8] The sharp band at 1716 cm^{-1}
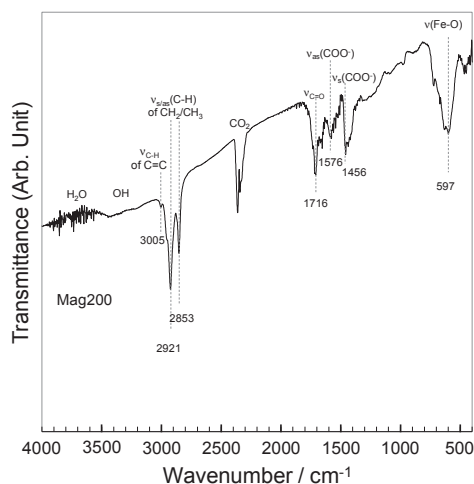
JCS-Japan

Makinose: Hydrothermal synthesis of near-monodisperse iron oxide nanoparticles using an ammonia-treated Fe-oleate precursor

Fig. 2. Representative FT-IR spectrum of a nanoparticle sample (Mag200) for identifying organic content.

Fig. 3. (Left column) Low-magnification (200,000×) TEM images of iron oxide nanoparticles synthesized at different temperatures. (Right column) High-magnification (600,000×) TEM images of the iron oxide nanoparticles synthesized at different temperatures.

corresponds to the stretching vibration of the C=O bond.[10] The band at $2400 \, cm^{-1}$ corresponds to CO_2, while the stretching of methyl and methylene are responsible for the sharp bands at 2853 and $2921 \, cm^{-1}$, respectively.[13] The small band at $3005 \, cm^{-1}$ corresponds to CH_2, specifically, the stretching vibration of the –CH=CH– double bond.[14] Finally, the noise in the $3500–4000 \, cm^{-1}$ range corresponds to H_2O. The above results confirm the presence of oleic acid and oleate groups in the iron oxide samples, with the COO^- vibrations indicating the formation of the oleate double-layer on the surfaces of the nanoparticles.[13]

Figures 3 and **4** show TEM and SAED images of the nanoparticle samples. Because of the hydrophobic nature of the oleate ligands on their surfaces, the dispersibility of the nanoparticles in cyclohexane was high for all the samples. The TEM images depict spherical particles with hexagonal faces, a geometry that is characteristic of that of previously reported iron oxide nanoparticles.[1,5] The SAED patterns corresponding to these images were identical to that of an Fe_3O_4 crystal, confirming the successful synthesis of crystalline iron oxide nanoparticles. With this hydrothermal synthesis technique, nanoparticle growth is controlled by Ostwald ripening. The size distributions of the samples were determined by collating the sizes of isolated (i.e., not agglomerated and under 12 nm in particle size) nanoparticles in the associated high-magnification TEM images. At least 500 particles were measured for each sample. The average particle sizes estimated from the TEM images are summarized in the graphs in Fig. 4, with the standard deviation defined as the error. The average sizes of the Mag200, Mag150, Mag100, and Mag80 samples were calculated to be 6.2, 5.2, 4.4, and 4.6 nm, respectively, with the CVs estimated as 17.1, 15.7, 20.7, and 22.3 %, respectively. These results suggest that a treatment temperature higher than 100 °C is required to obtain a distribution of nanoparticles with a low CV. The average interparticle distance of the Mag150 sample (the sample with the lowest CV) was calculated to be approximately
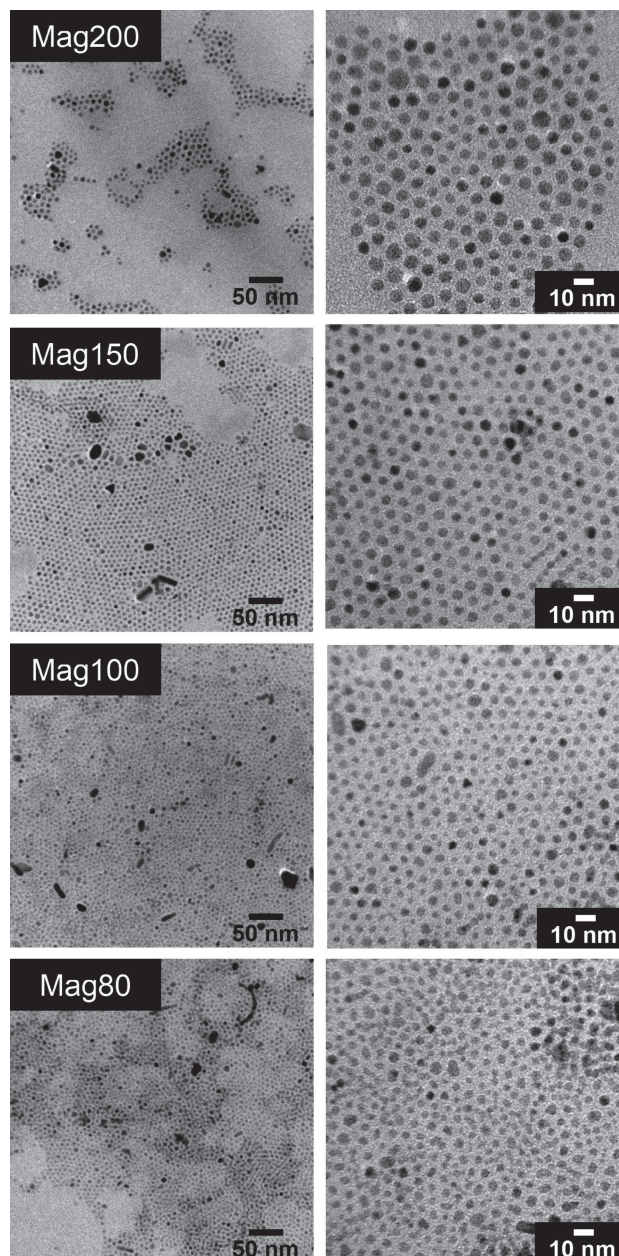
3.7 nm from the TEM images, while oleate groups are 2 nm long. These results thus suggest the creation of an oleate double-layer, in which the hydrophobic tails of the molecules in the second oleic acid layer (which are adsorbed on the iron oxide nanoparticles) penetrate the free tails of the molecules in the first oleate layer.

The size distribution of the nanoparticles in the liquid dispersion was measured using DLS, and the results (including average particle size and standard deviation) are shown in **Fig. 5**. Although, with this technique, the particle sizes obtained for each sample were larger than those
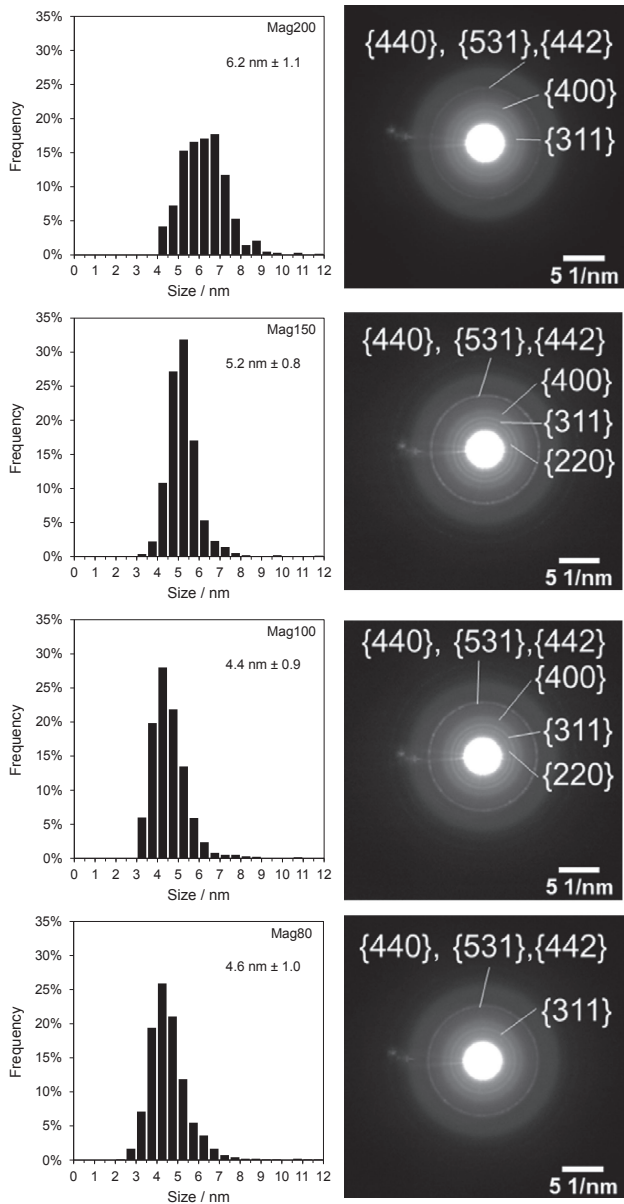
Fig. 4. (Left column) Size distributions of the nanoparticle samples obtained from the analysis of the high-magnification TEM images. At least 500 particles were counted to determine the particle size distribution of each sample. (Right column) The SAED patterns for the corresponding TEM images.
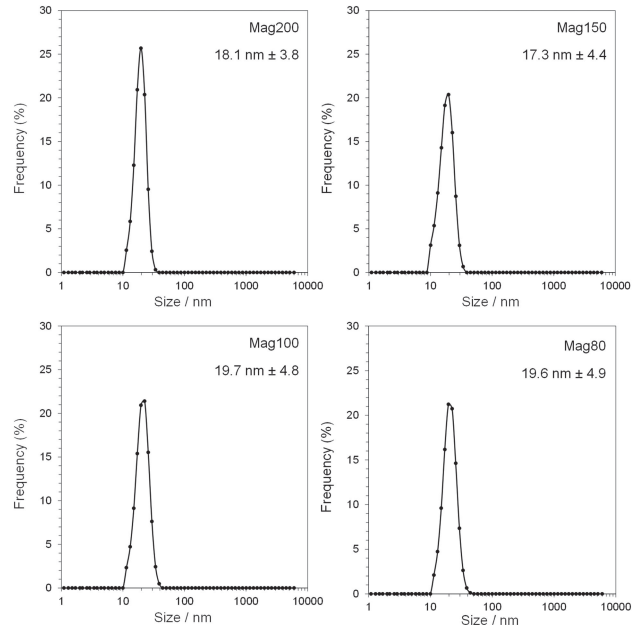

Fig. 5. Size distributions of the iron oxide nanoparticles synthesized at different temperatures, as obtained from DLS measurements.

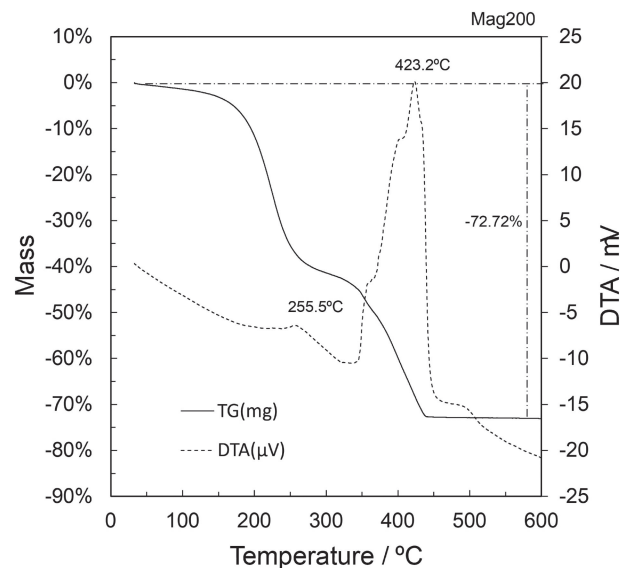Fig. 6. Representative TG–DTA curve of a nanoparticle sample (Mag200) for determining its concentration of organic content.

estimated using the TEM images, the trend for DLS to overestimate particle size in comparison to TEM measurement has been reported in previous studies.[7),11)]

Figure 6 depicts the TG–DTA curve of the Mag200 sample as a representative result of the investigation of the concentration of organic content in the nanoparticle dispersions. All TG–DTA curves exhibited similar features, with two steps observed in each curve. The first step (at approximately 250 °C) corresponds to oleate desorption from Fe-oleate in the iron oxide nanoparticles and its subsequent decomposition, while the second step (at approximately 420 °C) corresponds to free sodium oleate-like organic decomposition. This analysis revealed that the Mag200, Mag150, Mag100, and Mag80 samples con-

tained organic contents of 72.72, 69.92, 77.21, and 76.80 %, respectively.

Figure 7 shows the room-temperature magnetization of iron oxide nanoparticles obtained using the weights of the samples without organic content, which were calculated from the results of the TG–DTA analysis. The saturation magnetizations of Mag200, Mag150, Mag100, and Mag80 were estimated to be 77.0, 62.0, 50.1, and 44.9 emu/g, respectively. Here, it can be seen that the magnetization of the nanoparticles increased with the temperature used in hydrothermal processing. While these magnetization values are much smaller than those of bulk Fe_3O_4 (100
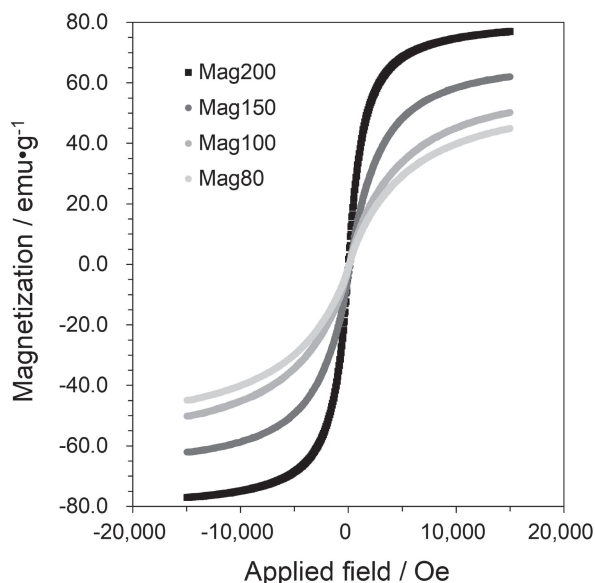
Fig. 7.   Room-temperature magnetization of iron oxide nano-particles synthesized at different temperatures.
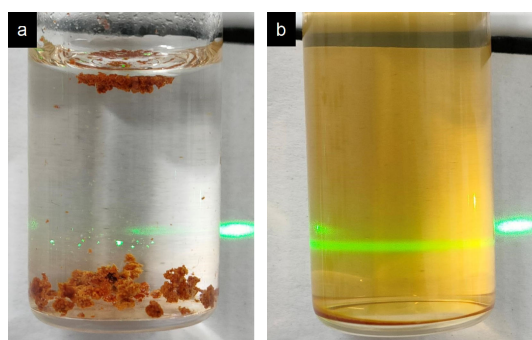

Fig. 8.   Dispersions of (a) Fe-oleate and (b) ammonia-treated Fe-oleate in water.

emu/g),[12] saturation magnetization values within the 30–80 emu/g range are consistent with those reported for iron oxide nanoparticles in the literature.[2),10),11),13),15)–17)]

4.   Discussion

Figure 8 compares the dispersions of Fe-oleate and ammonia-treated Fe-oleate in water. Although the Tyndall phenomenon was exhibited weakly in the Fe-oleate sample, it was clearly observed in the ammonia-treated Fe-oleate sample, indicating improved dispersion in the latter. The successful formation of nanoparticles with a narrow size distribution can thus be attributed to the uniform dispersion of their precursor in water. A detailed study focusing on nanoparticle generation and growth in this solution is required to clarify the exact mechanism through which ammonia treatment affects size distribution.

5.   Conclusion

In this study, iron oxide nanoparticles were synthesized from an ammonia-treated Fe-oleate precursor using a hydrothermal reaction performed at a range of temperatures. The nanoparticles had an inverse-spinel-type struc-ture and were capped with an oleate double-layer. The organic content of all the samples was approximately 70 %, with the average particle size ranging from 4.5–6.3 nm. The samples treated at 150 °C (Mag150) had the lowest CVs (15.7 %), suggesting that a treatment temperature of ∼150 °C is required for the synthesis of a sample of monodisperse nanoparticles. The saturation magnet-izations of all the nanoparticle samples were in the range of 44.9–77.0 emu/g, with Mag200 and Mag150 exhibiting the best magnetic performance.

References

1)   J. Park, K. An, Y. Hwang, J.-G. Park, H.-J. Noh, J.-Y. Kim, J.-H. Park, N.-M. Hwang and T. Hyeon, *Nat. Mater.*, **3**, 891–895 (2004).
2)   C.-J. Chen, H.-Y. Lai, C.-C. Lin, J.-S. Wang and R.-K. Chiang, *Nanoscale Res. Lett.*, **4**, 1343–1350 (2009).
3)   J. Xie, S. Peng, N. Brower, N. Pourmand, S. X. Wang and S. Sun, *Pure Appl. Chem.*, **78**, 1003–1014 (2006).
4)   A. Lassenberger, T. A. Grünewald, P. D. J. van Oostrum, H. Rennhofer, H. Amenitsch, R. Zirbs, H. C. Lichtenegger and E. Reimhult, *Chem. Mater.*, **29**, 4511–4522 (2017).
5)   L. M. Bronstein, X. Huang, J. Retrum, A. Schmucker, M. Pink, B. D. Stein and B. Dragnea, *Chem. Mater.*, **19**, 3624–3632 (2007).
6)   A. Stepanov, A. Mustafina, R. G. Mendes, M. H. Rümmeli, T. Gemming, E. Popova, I. Nizameev and M. Kadirov, *J. Iran. Chem. Soc.*, **13**, 299–305 (2016).
7)   J. Lim, S. P. Yeap, H. X. Che and S. C. Low, *Nanoscale Res. Lett.*, **8**, 381 (2013).
8)   T. Taniguchi, K. Nakagawa, T. Watanabe, N. Matsushita and M. Yoshimura, *J. Phys. Chem. C*, **113**, 839–843 (2009).
9)   C. A. Schneider, W. S. Rasband and K. W. Eliceiri, *Nat. Methods*, **9**, 671–675 (2012).
10)   D. Maity and D. C. Agrawal, *J. Magn. Magn. Mater.*, **308**, 46–55 (2007).
11)   K. El-Boubbou, R. O. Al-Kaysi, M. K. Al-Muhanna,

H. M. Bahhari, A. I. Al-Romaeh, N. Darwish, K. O. Al-Saad and S. D. Al-Suwaidan, *J. Nanomater.*, 2015, 620672 (2015).

12) A. G. Roca, J. F. Marco, M. del Puerto Morales and C. J. Serna, *J. Phys. Chem. C*, 111, 18577–18584 (2007).

13) X. Liang, X. Wang, J. Zhuang, Y. Chen, D. Wang and Y. Li, *Adv. Funct. Mater.*, 16, 1805–1813 (2006).

14) R. Zboril, A. Bakandritsos, M. Mashlan, V. Tzitzios, P. Dallas, C. Trapalis and D. Petridis, *Nanotechnology*, 19, 095602 (2008).

15) F. Ozel and H. Kockar, *J. Supercond. Nov. Magn.*, 30, 2023–2027 (2017).

16) K. Lee, S. Lee, M. C. Oh and B. Ahn, *Metals-Basel*, 8, 107 (2018).

17) W. Wu, Q. He and C. Jiang, *Nanoscale Res. Lett.*, 3, 397–415 (2008).